Design of passive ring resonators to be used for sensing applications

Caterina Ciminelli Dipartimento di Elettrotecnica ed Elettronica, Politecnico di Bari, Via Re David 200 – 70125 Bari, Italy
c.ciminelli@poliba.it

Carlo Edoardo Campanella Dipartimento di Elettrotecnica ed Elettronica, Politecnico di Bari, Via Re David 200 – 70125 Bari, Italy

Mario Nicola Armenise Dipartimento di Elettrotecnica ed Elettronica, Politecnico di Bari, Via Re David 200 – 70125 Bari, Italy

In this paper we report on the effects of two optical beams counterpropagating in a passive ring resonator that is the building block of several devices in a lot of sensing applications. By using the transfer matrix method in combination with the coupled mode theory, the analytical expressions of the power transfer functions for drop and through port configurations are derived in both cases of single beam and double beams inside the ring. The implemented model has shown some improvements in the resonator performance, such as the increase of the transmission power and the reduction of the linewidth, when the interaction between the two beams is considered, with respect to the single beam ring resonator configuration. [DOI: 10.2971/jeos.2009.09034]

Keywords: ring resonator, finesse, quality factor, sensors

1 INTRODUCTION

The ring resonator is an integrated optic structure with an optical feedback allowing a variety of functions such as wavelength filtering, optical switching or optical sensing. In [1]–[4] the behaviour of the ring resonator as a filter with an unidirectional power flow is described. In this work we report on an analytical model used to examine the interaction between the longitudinal modes of two counterpropagating beams. The analysis has been focused on the interaction between two counterpropagating beams having the same frequency. In this case the travelling wave (TW) beams, counterpropagating in the ring, generate a resonant standing wave (SW) that, in turn, couples with a pair of straight (bus) waveguides [5], as depicted in Figure 1. Differently from the single beam case, the coupler loses its spatial directionality and an evanescent standing mode is created in the coupling region, so generating two TWs in each bus waveguide.

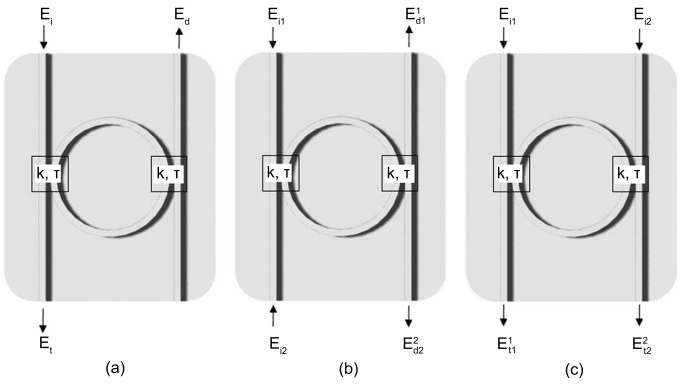

FIG. 1 (a) DSBC and TSBC, (b) DDBC, (c) TDBC.

The need of the pointed-out model to evaluate the performance of the ring resonator arises when the resonator is used, as an example, as sensing building block in a gyroscope.

2 METHODOLOGY

The ring resonator consists of a waveguide in a closed loop where only specific wavelengths can resonate. Two straight waveguides allow to couple the light into and out of the ring. The waveguide is a SiO_2/SiO_2:Ge/SiO_2/Si structure with a core size of few decades of μm^2 and under-cladding and over-cladding layers about 20 μm thick. The effective refractive index of the waveguide is 1.457, assuming an operating wavelength equal to 1550 nm.

The structure has been analyzed as a set of two coupled waveguides where E_i is the input field, E_t is the field at the through port, E_d is the field at the drop port and k and τ are, respectively, the coupling coefficient and the transmission coefficient between the straight waveguide and the ring waveguide, as it is shown in Figure 1(a). In particular, Figure 1 defines the configurations that can be considered assuming different input and output ports: drop port single beam configuration (DSBC) and through port single beam configuration (TSBC) (see Figure 1(a)); drop port double beams configuration (DDBC) (see Figure 1(b)) and through port double beams configuration (TDBC) (see Figure 1(c)).

The total ring length is $L_{TOT} = 0.144$ m. The delay time for a ring round trip is $T^* = L_{TOT}n/c \approx 0.7$ ns where c is the speed of light in vacuum, n is the waveguide effective refrac-

Received March 10, 2009; published June 26, 2009

tive index while the free spectral range is $FSR_{\Delta f} = 1/T^* \approx 1.43$ GHz or $FSR_{\Delta\lambda} = FSR_{\Delta f}\lambda_0^2/c \approx 11.45$ pm. Moreover, we assume the power loss α_i per unit length equal to 0.1 dB/cm and the coupler insertion loss $\beta = 0.2$ dB. A curvature radius of 2.3 cm allows neglecting the bending losses. We also assume a lossless coupling, i.e. $\tau = \sqrt{1-k^2}$.

By staggering the ring into a finite number of segments (see Figures 2 and 3), we can derive the transfer function of each segment for a co-propagating (progressive) wave, Eq. (1), and for a counterpropagating (regressive) wave, Eq. (2). The analytical model for the DDBC (Drop port Double Beams Configuration) is described in Section 2.1 by Eqs. (3)–(12), and for TDBC (Through port Double Beams Configuration) is reported in Section 2.2 (Eqs. (13)–(19)). Finally, in Section 3 we report on the numerical results and comment on that.

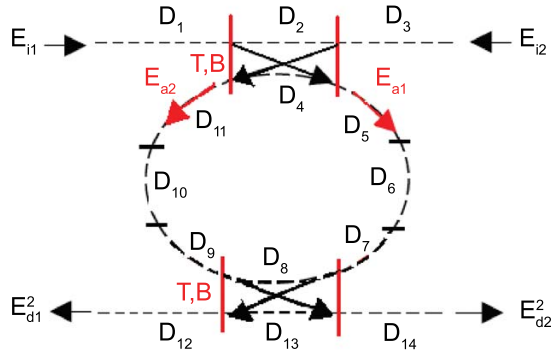

FIG. 2 Optical segmentation for the DDBC.

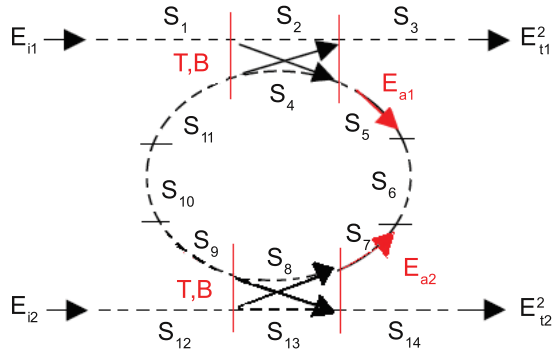

FIG. 3 Optical segmentation for the TDBC.

2.1 Drop port Double Beams Configuration (DDBC)

We used the transfer matrix method with boundary conditions obtained by applying the coupled mode theory, for achieving [6] the analytical expression of the power transfer function at the drop port with two counterpropagating laser beams, on the basis of the above assumptions.

As it is shown in Figure 2, we divided the full optical path into 14 segments: 8 segments within the ring and 3 segments for each bus waveguide. If L_i is the length of each segment D_i, the total ring length is given by $L_{RING} = L_4 + L_5 + L_6 + L_7 + L_8 + L_9 + L_{10} + L_{11} = 0.144$ m.

Due to the large curvature radius each curvilinear segment can be assumed to be linear. The transfer functions of the i-th segment for a co-propagating (progressive) wave, $D_i(\lambda)$, and for a counterpropagating (regressive) wave, $D_i^*(\lambda)$, are, respectively, expressed by the following equations:

$$D_i(\lambda) = e^{-\frac{\alpha_i}{2}} e^{-j\frac{2\pi}{\lambda} n_i L_i} \tag{1}$$

$$D_i^*(\lambda) = e^{-\frac{\alpha_i}{2}} e^{j\frac{2\pi}{\lambda} n_i L_i} \tag{2}$$

where α_i and n_i are the losses and the effective refractive index in each segment.

With reference to Figure 2, we are able to evaluate first the electric fields E_{a1} and E_{a2} within the ring, and, then, E_{d1} and E_{d2}, and the transfer function for the two counterpropagating beams configuration.

The field at the input of the segment D_5, E_{a1}, is given by:

$$E_{a1} = \frac{-jk\beta \prod_{i=1}^{2} D_i(\lambda)}{1 - \tau^2\beta^2 \prod_{i=4}^{11} D_i(\lambda)} E_{i1} \tag{3}$$

while the input field of the segment D_{11}, E_{a2}, is expressed by:

$$E_{a2} = \frac{-jk\beta \prod_{i=2}^{3} D_i^*(\lambda)}{1 - \tau^2\beta^2 \prod_{i=4}^{11} D_i^*(\lambda)} E_{i2} \tag{4}$$

In the DSBC the energy in the ring is supplied by an incident wave having an amplitude equal to E_{i1} (respectively E_{i2}). The output is the detected wave E_{d1}^1 (respectively, E_{d2}^1). The TW supported by this configuration has amplitude E_{a1} (respectively, E_{a2}) which can be normalized with respect to E_{i1} (respectively, E_{i2}), so obtaining $|E_{a1}/E_{i1}|^2$ (respectively, $|E_{a2}/E_{i2}|^2$) which represents the total normalized power flowing through any cross section of the ring waveguide.

In the DDBC and TDBC the energy in the ring is supplied by two counterpropagating incident waves of amplitude E_{i1} and E_{i2}. If we consider the same output port of the DSBC, the output is represented by the detected wave E_{d1}^2 whereas if we consider the output port on the same waveguide in opposite direction the output is E_{d2}^2.

The DDBC and TDBC support two counterpropagating TWs which, after a transient, generate a resonant SW with a amplitude which is a linear combination of E_{a1} and E_{a2}.

The expression of the drop transfer function for the single beam configuration can be compared to those ones for the double beams case.

By using Eqs. (3) and (4), we obtain the field expressions when the two output ports are assumed on the same waveguide:

$$E_{d1}^1 = -jk\beta \left[D_{12}(\lambda) \prod_{i=5}^{8} D_i(\lambda) E_{a1} \right] \tag{5}$$

$$E_{d2}^1 = -jk\beta \left[D_{14}^*(\lambda) \prod_{i=8}^{11} D_i^*(\lambda) E_{a2} \right] \tag{6}$$

The complete expression of the field at both drop ports is derived in the DDBC, using Eqs. (5) and (6), by taking into ac-

count the interference occurring between the counterpropagating fields, leading to a standing wave within the ring resonator:

$$E_{d1}^2 = E_{d2}^2 = -jk\beta \left[D_{12}(\lambda) \prod_{i=5}^{8} D_i(\lambda) E_{a1} + D_{14}^*(\lambda) \prod_{i=8}^{11} D_i^*(\lambda) E_{a2} \right] \quad (7)$$

where the term into the square brackets represents the resonant standing wave within the ring resonator as linear combination of E_{a1} and E_{a2}.

E_{a1} and E_{a2} have the same starting points so, as it can be seen from Figure 2, they start to interfere in S_8, that is the coupling region of lower evanescent coupler, after they have covered a phase shift of π opposite in sign; this means a totally phase shift between the two counterpropagating waves of 2π. So, in the phase domain the resonant standing wave will reach the maximum value when the phase shift is $2\pi + 2m\pi$ and the constructive interference will occur for any m, integer multiple of π.

In matrix form we can rewrite E_{d1}^2 and E_{d2}^2 as functions of the two counterpropagating incident waves of amplitude E_{i1} and E_{i2}:

$$\begin{bmatrix} E_{d1}^2 \\ E_{d2}^2 \end{bmatrix} = (-jk\beta)^2 \begin{bmatrix} \frac{N_{aa}}{D_{aa}} & \frac{N_{ab}}{D_{ab}} \\ \frac{N_{ba}}{D_{ba}} & \frac{N_{bb}}{D_{bb}} \end{bmatrix} \begin{bmatrix} E_{i1} \\ E_{i2} \end{bmatrix} \quad (8)$$

where:

$$\frac{N_{aa}}{D_{aa}} = \frac{N_{ba}}{D_{ba}} = D_{12}(\lambda) \prod_{i=5}^{8} D_i(\lambda) \frac{\prod_{i=1}^{2} D_i(\lambda)}{1 - \tau^2\beta^2 \prod_{i=4}^{11} D_i(\lambda)} \quad (9)$$

$$\frac{N_{bb}}{D_{bb}} = \frac{N_{ab}}{D_{ab}} = D_{14}^*(\lambda) \prod_{i=8}^{11} D_i^*(\lambda) \frac{\prod_{i=2}^{3} D_i^*(\lambda)}{1 - \tau^2\beta^2 \prod_{i=4}^{11} D_i^*(\lambda)} \quad (10)$$

Eqs. (9) and (10) are the DSBC transfer functions, referred to the inputs E_{i1} and E_{i2}, respectively.

By imposing $E_{i1} = E_{i2} = E_i$, we obtain the power transfer function at both drop ports expressed by the following equations:

$$\frac{|E_{d1}^2|^2}{|E_i|^2} = (-jk\beta)^4 \frac{|N_{aa}D_{ab} + N_{ab}D_{aa}|^2}{|D_{aa}D_{ab}|^2} \quad (11)$$

$$\frac{|E_{d2}^2|^2}{|E_i|^2} = (-jk\beta)^4 \frac{|N_{bb}D_{ba} + N_{ba}D_{bb}|^2}{|D_{bb}D_{ba}|^2} \quad (12)$$

2.2 Through Drop Double Beams Configuration (TDBC)

By following the same procedure as in Section 2.1, we found the analytical expression of the power transfer function at the through port for the configuration in Figure 1(c), again using the same segmentation technique, as in Figure 3.

We obtain

$$\begin{bmatrix} E_{t1}^2 \\ E_{t2}^2 \end{bmatrix} = \begin{bmatrix} \frac{N_{cc}}{D_{cc}} & \frac{N_{cd}}{D_{cd}} \\ \frac{N_{dc}}{D_{dc}} & \frac{N_{dd}}{D_{dd}} \end{bmatrix} \begin{bmatrix} E_{i1} \\ E_{i2} \end{bmatrix} \quad (13)$$

where:

$$\frac{N_{cc}}{D_{cc}} = \tau\beta \prod_{i=1}^{3} D_i(\lambda) + (-jk\beta)^2 \beta\tau \frac{\prod_{i=1}^{11} D_i(\lambda)}{1 - \tau^2\beta^2 \prod_{i=4}^{11} D_i(\lambda)} \quad (14)$$

$$\frac{N_{cd}}{D_{cd}} = (-jk\beta)^2 \prod_{i=4}^{7} D_i^*(\lambda) \frac{\prod_{i=2}^{3} D_i(\lambda) \prod_{i=12}^{13} D_i^*(\lambda)}{1 - \tau^2\beta^2 \prod_{i=4}^{11} D_i^*(\lambda)} \quad (15)$$

$$\frac{N_{dc}}{D_{dc}} = (-jk\beta)^2 \prod_{i=1}^{2} D_i(\lambda) \frac{\prod_{i=13}^{14} D_i^*(\lambda) \prod_{i=5}^{8} D_i(\lambda)}{1 - \tau^2\beta^2 \prod_{i=4}^{11} D_i(\lambda)} \quad (16)$$

$$\frac{N_{dd}}{D_{dd}} = \tau\beta \prod_{i=12}^{14} D_i(\lambda) + (-jk\beta)^2 \beta\tau \frac{\prod_{i=4}^{14} D_i^*(\lambda)}{1 - \tau^2\beta^2 \prod_{i=4}^{11} D_i^*(\lambda)} \quad (17)$$

If we put $E_{i1} = E_{i2} = E_i$, we obtain the power transfer function at each through port:

$$\frac{|E_{t1}^2|^2}{|E_i|^2} = \frac{|N_{cc}D_{cd} + N_{cd}D_{cc}|^2}{|D_{cc}D_{cd}|^2} \quad (18)$$

$$\frac{|E_{t2}^2|^2}{|E_i|^2} = \frac{|N_{dd}D_{dc} + N_{dc}D_{dd}|^2}{|D_{dd}D_{dc}|^2} \quad (19)$$

If we suppose an initial phase shift between the counterpropagating fields so that:

$$E_{i1} = E_i \quad E_{i2} = E_i e^{j\Phi} \quad (20)$$

we obtained the power transfer functions at both drop ports as expressed by Eqs. (21) and (22):

$$\frac{|E_{d1}^2|^2}{|E_i|^2} = (-jk\beta)^4 \frac{|N_{aa}D_{ab} + N_{ab}D_{aa}e^{j\Phi}|^2}{|D_{aa}D_{ab}|^2} \quad (21)$$

$$\frac{|E_{d2}^2|^2}{|E_i|^2} = (jk\beta)^4 \frac{|N_{bb}D_{ba}e^{j\Phi} + N_{ba}D_{bb}|^2}{|D_{bb}D_{ba}|^2} \quad (22)$$

and the power transfer functions at the through ports as:

$$\frac{|E_{t1}^1|^2}{|E_i|^2} = \frac{|N_{cc}D_{cd} + N_{cd}D_{cc}e^{j\Phi}|^2}{|D_{cc}D_{cd}|^2} \quad (23)$$

$$\frac{|E_{t2}^2|^2}{|E_i|^2} = \frac{|N_{dd}D_{dc}e^{j\Phi} + N_{dc}D_{dd}|^2}{|D_{dd}D_{dc}|^2} \quad (24)$$

3 NUMERICAL RESULTS

Figure 4 compares the shape of the power transfer function for the DDBC (black), expressed by Eq. (7) with $\Phi = 0$, to that one of the DSBC (grey), expressed by Eq. (5). Propagation loss is assumed equal to 0.1 dB/cm, the coupler insertion loss is 0.2 dB and $K = 0.03$, where $K = k^2$ is the power coupling coefficient. Figure 4 clearly shows the improvement of the performance for the DDBC in terms of reduction of the Full Width at Half Maximum (FWHM) and of enhancement of the power peak.

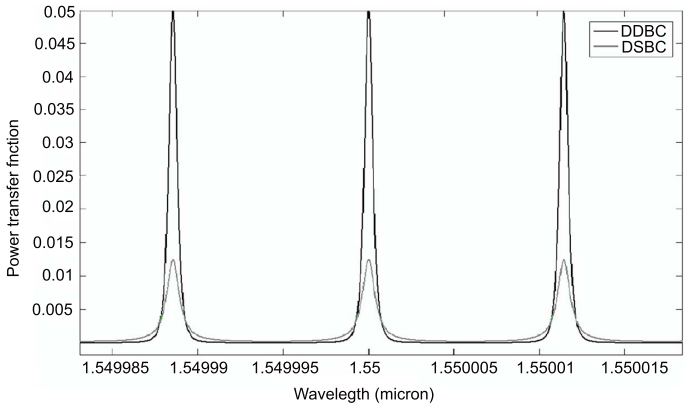

FIG. 4 DDBC power transfer function (black) versus λ for K = 0.03 compared with DSBC (grey).

Parameter	DDBC	DSBC
FWHM [MHz]	75	110
Finesse	15.5	10
Quality factor	9×10^5	2×10^5

TABLE 1 Comparison of the resonator parameters Δf = 0, λ = 1.55 μm

Parameter	TDBC	TSBC
FWHM [MHz]	40	60
Finesse	29	18
Quality factor	$1,7 \times 10^6$	$3,6 \times 10^5$

TABLE 2 Comparison of the through port resonator parameters Δf = 0, λ = 1.55 μm

When the two counterpropagating beams are shifted by $\Phi = -2\pi \cdot \Delta\lambda nL/\lambda\lambda_1 \approx -2\pi \cdot \Delta\lambda nL/\lambda^2$ with $\Delta\lambda = -\Delta f\lambda_0^2/c$ and $\lambda_1 = \lambda + \Delta\lambda$ the resulting wave within the ring is a quasi-standing wave.

In Figure 5 the transfer function expressed by Eq. (11) has been plotted for $\Delta f = 0$ and for different values of Δf. A shift even small between the two counterpropagating beams induces a splitting of the resonant peak, with the second peak appearing at the same wavelength of the resonance for the case with $\Delta f = 0$. The distance between the two peaks increases proportionally to Δf. Furthermore, the power value of the resonance is strongly reduced with respect to the case without any phase shift when Δf increases from 0 to 2 MHz, while it remains quite constant when Δf is further increased.

The comparison between DDBC and DSBC also in terms of FWHM, Finesse and Quality Factor is summarized in Table 1.

As in the drop configuration case, Figure 6 reports the comparison between the power transfer function for the through port double counterpropagating beams (black) and the power transfer function for the through port single beam configuration (grey). The peculiar behaviour obtained in case of double beams is caused by an effect similar to the Vernier one: the difference in optical path lengths, equal to a half ring length, between the counterpropagating beams creates a phase-shift that partially suppresses the odd resonant mode, obtaining a free spectral range (FSR) enlarged by π. In particular, we have demonstrated a partial suppression of the odd longitudinal modes for this particular value of K.

In Figure 6, by plotting Eq. (23) for $K = 0.03$, the performance improvement, with respect to the TSBC, appears only for the even resonant modes.

Figure 7 illustrates the behaviour of the resonator with a TDB configuration when Δf assumes different values, i.e.$\Delta f = 0$, 2, 4 and 6 MHz. In this figure, it can be observed that the significant improvement of the power transfer function for the TDB configuration with respect to the single beam case, as in Figure 6, is lost when Δf is non null, at either odd or even resonant wavelengths.

In Table 2 a comparison of the calculated values of FWHM, finesse and quality factor for the TDBC and TSBC is reported. As it can be observed best values of those performance parameters are obtained in the TDBC.

For the drop geometry, in presence of two counterpropagating beams, assuming the beams at same frequency, we have calculated better performance, in terms of FWHM, finesse, and Q-factor, with respect to the drop single beam configuration.

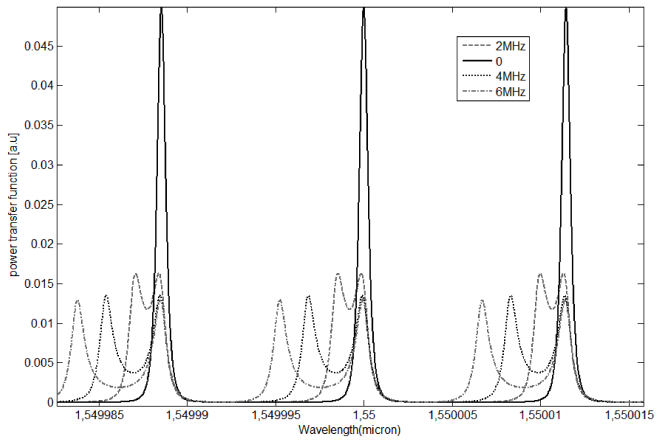

FIG. 5 DDBC power transfer function (black) for different value of Δf.

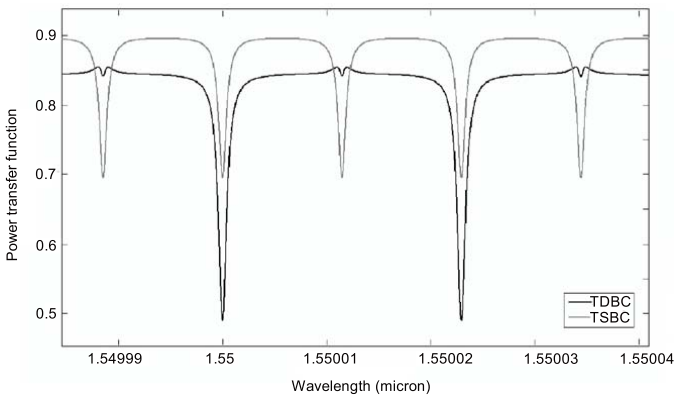

FIG. 6 TDBC power transfer function (black) versus λ for K = 0.03 compared with TSBC (grey).

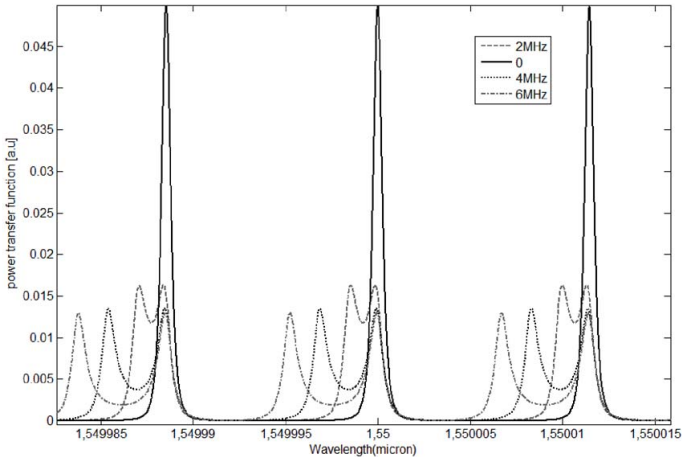

FIG. 7 TDBC power transfer function for different values of Δf.

Same situation has been observed also for the through port configurations. For the TDB case, the transfer function does not have the peaks corresponding to the odd resonant wavelengths, due to Vernier effects, while for TSB case a significant reduction of the amplitude of the transfer function results.

By comparing the design parameter values for the TDBC with those for DDBC, one can derive best design conditions for the through port configuration using two counterpropagating beams.

4 CONCLUSIONS

In this work we have studied the effect of coupling of two counterpropagating beams in a waveguiding ring resonator. The aim of this study was to search both best configuration and best operating condition for a high performance sensitive element to be used as building block of sensing devices, e.g. angular velocity sensors. A better performance of drop double beam configuration due to the reduction of the FWHM, to the enhancement of the power peaks, to the increase of the quality factor and finesse has been demonstrated with respect to the drop single beam case.

References

[1] L. N. Binh, N. Q. Ngo, and S. F. Luk, "Graphical Representation and Analysis of the Z-Shaped Double-Coupler Optical Resonator" IEEE J. Lightwave Technol. **11**, 1782–1792, (1993).

[2] C. J. Kaalund and G. D. Peng, "Pole-Zero Diagram Approach to the Design of Ring Resonator-Based Filters for Photonic Applications" IEEE J. Lightwave Technol. **22**, 1548–1559, (2004).

[3] R. Grover, P. P. Absil, T. A. Ibrahim, and P. T. Ho, *III-V Semiconductor Optical Micro-Ring Resonators* 110–129 (Proceedings of AIP Conference, International School of Quantum Electronics, 39th Course **709**, 2004).

[4] C. K. Madsen and J. H. Zhao, *Optical Filter design and analysis* (Wiley Inter-Science, 1999).

[5] M. A. Popovic, C. Manolatou, and M. R. Watts, "Coupled_induced resonance frequency shifts in coupled dielectric multi-cavity filters" Opt. Express **14**, 1208–1222 (2006).

[6] C. Ciminelli, C. E. Campanella, and M. N. Armenise, "Optimized Design of Integrated Optical Angular Velocity Sensors based on a Passive Ring Resonator" to be published in IEEE J. Lightwave Technol. (2009).